frontiers | Frontiers in Climate

TYPE Original Research
PUBLISHED 18 December 2024
DOI 10.3389/fclim.2024.1408038

OPEN ACCESS

EDITED BY
Eduardo Siegle,
University of São Paulo, Brazil

REVIEWED BY
Alejandro López-Ruiz,
University of Seville, Spain
Julia Reid,
University of São Paulo, Brazil

*CORRESPONDENCE
Giorgia Verri
✉ giorgia.verri@cmcc.it

RECEIVED 27 March 2024
ACCEPTED 11 November 2024
PUBLISHED 18 December 2024

CITATION
Verri G, De Lorenzis A, Santos da Costa V, Sorolla A, Löchner A, Ribot M, Marti E, DelGado SC, Coppini G and Pinardi N (2024) Salt-wedge estuary's response to rising sea level, reduced discharge, and Nature-Based Solution. *Front. Clim.* 6:1408038. doi: 10.3389/fclim.2024.1408038

Salt-wedge estuary's response to rising sea level, reduced discharge, and Nature-Based Solution

Giorgia Verri[1]*, Alessandro De Lorenzis[1], Vladimir Santos da Costa[1], Albert Sorolla[2], Adrian Löchner[2], Miquel Ribot[3], Eugenia Marti[3], Sara Castelar DelGado[3], Giovanni Coppini[1] and Nadia Pinardi[4]

[1]CMCC Foundation - Euro-Mediterranean Center on Climate Change, Lecce, Italy, [2]NATURALEA, Barcelona, Spain, [3]Center for Advanced Studies of Blanes, CEAB-CSIC, Barcelona, Spain, [4]Department of Physics and Astronomy, University of Bologna, Bologna, Italy

Vulnerable estuaries face resilience challenges against climate-induced salinization. This study examines the Po di Goro estuary in the Northern Adriatic Sea using an innovative modeling approach. It assesses the effectiveness of a Nature-Based Solution in reducing the threat of salt-wedge intrusion. An intermediate-complexity numerical model is considered, leveraging its low computational cost, which is suitable for climate projections, along with robust physics encompassing the main estuarine processes. Two centennial climate experiments covering 1991–2100 are proposed following a mechanistic modeling approach to understand the compound effects of sea level rise and river discharge changes. The first experiment is a full forcing experiment. The second experiment uses the same model but removes the sea level rise as an input forcing. A third experiment, referred to as the Digital Twin Experiment, assesses the effectiveness of a location-specific Nature-Based Solution. This experiment specifically examines the impact of reducing salt levels in the water by using a halophyte plant along the estuary. The results show that, in a future climate change scenario, the salt-wedge intrusion increases. This response is due to the non-linear combination of reduced river discharge and the local sea level rise. The discharge decrease acts as the main driver in the mid-term future (i.e., 2050–2080). In the long-term future (i.e., 2080–2100), the local sea level rise becomes more relevant as the discharge trend is expected to be null. The salt-wedge intrusion in the Po di Goro is projected to increase up to 63% annually (120% in summertime). Additionally, the river mouth salinity could rise by 27% annually (69% in summertime) in the long-term future (2081–2100). The halophyte plant, Atriplex portulaciodes, proposed as Nature-Based Solution, could reduce salt-wedge intrusion in the Po di Goro by up to 16% annually (22% in summer) in the long-term future. In the short-term future, this Nature-Based Solution may be effective enough to counteract the salt increase.

KEYWORDS

river-dominated estuary, local sea level rise, river discharge decrease, salt-wedge intrusion, two-layer estuary box model, Nature-Based Solution

1 Introduction

Estuarine transitional zones are highly vulnerable coastal areas to the changing climate. Historical and future trends of streamflow at global and regional scales indicate that the river discharge is expected to decrease in Europe, the Middle East, southwestern United States, and Central America, with a particularly severe decrease affecting the rivers entering the Mediterranean Sea (Koirala et al., 2014; Lee et al., 2024). Additionally, the total sea level is projected to rise both globally and regionally, including in the Mediterranean basin (Pörtner et al., 2022; Ablain et al., 2019; Storto et al., 2019; Sannino et al., 2022). However, a few recent studies, which provide historical reconstructions and/or future projections of the sea level at very local scales, demonstrate the heterogeneous behavior of the Mediterranean sea level rise. This varies by time and location, with some coastal areas experiencing a decrease in sea level (Meli et al., 2023; Verri et al., 2024; Borile et al., 2024 under review). Overall, the river discharge decrease, RDD, and/or the local sea level rise, SLR, contribute to (i) a persistent increase in the salt content of surface and subsurface catchment waters and (ii) an increase in salt-wedge intrusion (SWI), even in unmodified natural river systems. SWI is exacerbated in shallow estuaries (Prandle and Lane, 2015), in catchments subject to water regulations (Little et al., 2016), and in storm surge-impacted areas. Moreover, the increase in SWI is highly non-linear (Krvavica and Ružić, 2020) and varies under the combined effect of its preconditioning factors and their evolution in a changing climate. These factors include the local geometry, tidal range, runoff regime, and total sea level. Changes in SWI threaten the survival of the fragile estuarine ecosystems and imply increasing damage to agriculture, drinking water supply, and the ecosystem services that estuaries provide. In the past decade, numerous studies have investigated the preconditioning factors that control the SWI along the estuaries. The general conclusion is that the river discharge plays the dominant role, followed by the sea level which may prevail for seasonal variations. Channel geometry and local winds may also play significant roles (Tian, 2019). However, estuarine dynamics and its main stressors include a vast range of conditions, making generalization of results difficult (Geyer and MacCready, 2014). Most literature studies have focused on well-mixed estuaries under macro-tidal conditions. Salt-wedge estuaries (Valle Levinson, 2010), which are highly stratified estuaries and end in micro-tidal seas, are still poorly investigated. Consequently, the role of SLR in these estuaries, in conjunction with RDD (Krvavica and Ružić, 2020), is unclear. For instance, Prandle and Lane (2015) investigated a large sample of UK estuaries and concluded that the shallower ones with depths <10 m, flowing into a micro-tidal sea, exhibit a significant role of SLR on SWI length. Only a few studies, such as those by Tsz Yeung Leung et al. (2018) and Bellafiore et al. (2021), have analyzed SWI projections under climate conditions. This is partially justified by the fact that the SLR close to the river mouths is still highly uncertain. A source of uncertainty in SLR is represented by the limitations of the available climate scenarios (Adloff et al., 2018), which generally cover only regional scales and simplify or neglect connections among Earth system components (Holt et al., 2017).

Recent efforts are aimed at proposing regional-to-local climate downscaling, using both dynamical and statistical approaches. This is done to provide reliable scenarios with integrated modeling systems and high temporal and spatial details (Drenkard et al., 2021; Holt et al., 2022; Denamiel and Vilibić, 2023; Verri et al., 2024). Another challenge is that accurate long-term projections of local SLR in the estuary-sea continuum require high-resolution numerical models. Such models can realistically represent the complex geometry and cross-scale processes of estuaries and shelf seas but require extensive calibration and significant computational resources.

For all these reasons, a digital tool should be set up to simulate specific river estuaries, determining the compounding effects that produce changes in SWI. The numerical modeling framework should be capable of simulating centennial timescales and be adaptable to diverse estuarine conditions. With this purpose, the current study uses a one-dimensional, two-layer estuary box model, known as the CMCC EBM (Verri et al., 2020, 2021). It solves the estuarine water exchange through two conservation equations for volume and salt, averaged over the diurnal tidal cycle, and employs two parametric equations to estimate the SWI length and the along-estuary mixing. The EBM has been applied to the Po di Goro branch of the Po river delta system. Its estuary is river-dominated and flows into the micro-tidal Northern Adriatic Sea. The selected case study is increasingly affected by inland water salinization, impacting agriculture and other economic activities (Colombani et al., 2016). Tarolli et al. (2023) identified the Po delta area as one of the primary global hotspots for salt-wedge intrusion.

This study primarily addresses the knowledge gap regarding the compounding effects of RDD and SLR on salt intrusion dynamics. The EBM tool enables centennial climate projections using a deterministic approach, revealing how RDD and local SLR combine in a non-linear way to increase the SWI. The secondary aim of this study is to evaluate the effectiveness of a Nature-Based Solution NBS (Cohen-Schacham et al., 2016; Gallotti et al., 2021) using a Digital Twin approach (Pillai et al., 2022). By leveraging on a model validated for present climate conditions, two experiments are designed to demonstrate the compounding effects of SLR and RDD. Our third experiment explores the potential of a site-specific NBS, a halophyte plant, to mitigate increasing SWI. Section 2 describes the study area, modeling methodology, and experimental setup. Section 3 analyzes the numerical results, and conclusion is presented in Section 4.

2 Method

2.1 The study site

The Po di Goro is a branch, ~45 km long, of the Po river delta system (Figure 1). Its estuary conveys ~13% of the runoff

Abbreviations: ISS, inflowing sea salinity; RDD, river discharge decrease; SLR, sea level rise; SWI, salt-wedge intrusion; NBS, nature-based solution; EBM, estuary box model; RCM, regional climate model; RCP, representative concentration pathway; TSL, total sea level.

FIGURE 1
Map of the Po delta system (Google Earth image) and the river mouths, that are, Po di Maistra, Po della Pila (which splits into Po di Tramontana, Po di Dritta, Po di Scirocco, Po di Bonifazi and Po di Bastimento), Po di Tolle, Po di Gnocca, and Po di Goro (yellow markers). The red path, with specified head and mouth coordinates, is the Po di Goro branch selected as the test case. The geographical area where Po delta system is located is shown in the left inset.

of the Po river which is the second freshwater source of the Mediterranean Sea. The Po di Goro branch is linked to the Goro Lagoon through multiple connections regulated by sluice gates and locks. The Goro Lagoon is the largest water body of the delta, and it is also the one with the highest aquaculture activities (Carafa et al., 2006). The Po di Goro estuary is a salt-wedge estuary, i.e., a river-dominated estuary ending into the micro-tidal Northern Adriatic Sea. It has a persistent high discharge in autumn and spring and a minimum discharge during summer, reaching its lowest point in August. The low tidal range makes this estuary generally stratified with a salt wedge. This wedge can advance more than 20 km when moderate-to-low runoff occurs i.e., in summer time (Verri et al., 2021). Although the SWI has been investigated under climate change by including the natural drivers such as sea level, river discharge, and heat fluxes (Bellafiore et al., 2021), there is still a large uncertainty about the human interventions, such as channel deepening, dams building, irrigation and agriculture (Tarolli et al., 2023) and, more generally, land use changes (Corbau et al., 2019). Past and present monitoring observations show this estuary is experiencing: (i) a decrease in discharge, (ii) an increase in SWI. Kurdistani et al. (2022) and Bellafiore et al. (2021) provided future projections of SWI for the Po di Goro river as well as the whole Po delta system. These projectons indicate the SWI will exacerbate under changing climate scenarios.

2.2 Experimental design

2.2.1 The estuary intermediate-complexity model

The CMCC EBM is an intermediate-complexity 2-layer estuary box model that links the riverine freshwater discharge and the marine salt water and solves the estuarine water exchange averaged over the diurnal tidal cycle. The estuary volume is assumed to be a rectangular box with constant width L_y. The estuary length L_x represents the salt-wedge intrusion (SWI) length, and it is a time-dependent parameter in the equations. The estuary box has only two open boundaries at the head and mouth of the estuary. To simulate a two-layer exchange flow, the water exchange is discretized only vertically. Water enters through both layers at the cross sections of the estuary head and mouth, while it exits only through the upper layer at the estuary mouth cross section. This EBM setting neglects evaporation and precipitation rates at the top surface of the estuary box. This is a reasonable assumption for most estuaries, including the Po delta, where runoff typically dominates the freshwater budget. However, there are a few exceptions, named "inverse estuaries" where evaporation and precipitation are the primary drivers of circulation (Lorenz et al., 2021). The equations of the model are averaged over the diurnal tidal cycle, which includes both the ebb and flood tidal phases, i.e., the seaward and landward tidal pumping, respectively, making it reasonable to assume a two-layer exchange flow dynamics.

Input fields are the river inflow or discharge with zero salinity at the estuary head and the level $H_{tot} = H_{bathy} + TSL$, where H_{bathy} is the estuary mouth depth and TSL is the local total sea level at the river mouth. The sea water inflow at the river mouth includes the baroclinic inflow through the bottom layer and the tidally driven barotropic one through the whole water column. The inflow salinity in the lower layer is also specified.

The EBM output fields include the net outflowing volume flux, the salinity at the estuary mouth, the SWI length, and the along-estuary horizontal diffusivity. A sketch of the estuary box, including the input and output fields, is provided in Figure 2.

The model includes two conservation equations for the volume flux and the salt flux which are written under steady state and incompressible fluid hypotheses and averaged over the diurnal tidal cycle. They provide the outflowing volume flux, Q_{ul}, and salinity, S_{ul}, at the river mouth which are read as below:

$$Q_{ul} = Q_{river} + Q_{ll} + Q_{tidef} \tag{1}$$

$$S_{ul}Q_{ul} = S_{ll}Q_{ll} + S_{ocean}Q_{tidef} + K_{SH}H_{tot}L_y\frac{S_{ocean}}{L_x} \tag{2}$$

where subscripts ul and ll refer to the upper and lower layer. The $Q_{ll} = u_{ll}L_y\frac{H_{tot}}{2}$ and S_{ll} are the baroclinic inflowing volume flux and salinity at river mouth. The river volume flux or discharge, $Q_{river} = u_{river}L_yH_{tot}$, is provided at the estuary head, i.e., at the last section along the river network moving in the downstream direction where the salinity is still equal to zero on multi-year average conditions. The $Q_{tidef} = L_yH_{tot}u_{tidef}$ and u_{tidef} are the barotropic inflowing volume flux and velocity corresponding to the flood tide phase, S_{ocean} is the depth averaged ocean salinity at river mouth. The coefficient $K_{SH} = C_kL_yu_{tidef}$ is the horizontal along-estuary diffusivity where C_k is the non-dimensional coefficient representative of the estuary stratification. In a previous study (Verri et al., 2021), we presented a parametric equation to determine C_k by means of a dimensional analysis using the theorem of Buckingham and Self-Similarity (Barenblatt, 1987; Kurdistani et al., 2019). The literature shows a wide range of values for C_k, from $\mathcal{O}(10^{-2})$ to $\mathcal{O}(10^2)$ (MacCready, 2004). The dimensional equation for C_k, calibrated for the Po di Goro estuary, reads as below:

$$C_k = \begin{cases} 200(\frac{\rho_{ll}}{\rho_{river}})^{20}(\frac{Q_{tidef}}{Q_{river}})^{0.1}e^{-2000(F_t^2\frac{L_y}{H_{tot}})}, & \text{if } Q_{river} < \overline{Q_{river}} \\ (\frac{\rho_{ll}}{\rho_{river}})^{20}(\frac{Q_{tidef}}{Q_{river}})^{-0.5}e^{-2000(F_t^2\frac{L_y}{H_{tot}})}, & \text{if } Q_{river} \geq \overline{Q_{river}} \end{cases} \tag{3}$$

where $F_t = \frac{u_{tidef}}{\sqrt{gH_{tot}}}$ is the tidal Froude number, $\rho_{river} = 1000 kgm^{-3}$ is the river freshwater density, $\rho_{ll} = \rho_0(1 + k_sS_{ll})$ is the lower layer density with the haline contraction coefficient taken to be constant and equal to $k_s = 7.7 \times 10^{-4} psu^{-1}$, and $\overline{Q_{river}}$ is the multiannual averaged runoff. It has been found that the river volume flux Q_{river} is the main input parameter that governs the estuary stratification and the balance in dimensional (Equation 3).

Similarly, the estuary length L_x follows a parametric equation developed by Verri et al. (2021) using the dimensional analysis with a list of coefficients to be tuned for the target estuary. It reads as below:

$$L_x = 0.019H_{tot}F_r^{-0.673}(\frac{\rho_{ll}}{\rho_{river}})^{108.92}(\frac{Q_{tidef}}{Q_{river}})^{0.075}(\frac{Q_{ll}}{Q_{river}})^{-0.0098} \tag{4}$$

where $F_r = \frac{u_{river}}{\sqrt{gH_{tot}}}$ is the river Froude number. A detailed demonstration of the EBM equations can be found in Verri et al. (2020, 2021). For the study case of the Po di Goro estuary, a multivariate regression technique was applied to determine the tunable coefficients of the dimensional (Equations 3, 4).

The EBM has already been successfully applied to the Po di Goro branch. The calibration of the tunable coefficients and the validation of the modeling results for the specific case study are reported in Verri et al. (2021). Previous studies using the EBM have demonstrated (i) the effectiveness of the box modeling approach for studying the estuarine water exchange and (ii) the EBM features that make it particularly suitable for climate applications. Furthermore, the simple channel geometry of the Po di Goro, with an almost null bed slope and no meanders, makes the current EBM configuration especially suitable for modeling this salt-wedge estuary. The EBM offers low computational and data-storage costs compared to the 3D high-resolution numerical models which are required to represent complex estuary geometries (Verri et al., 2023). The EBM is grid agnostic, eliminating the need for a detailed knowledge of the local bathymetry which may be unknown or uncertain. Furthermore, the model physics encompasses most key estuarine dynamic processes, which are either explicitly solved or parameterized.

Despite the strengths of the EBM, certain limitations remain. First, the assumption of two vertical layers of equal thickness at the river mouth is a simplification. In reality, the daily average net outflow at the top of the estuary mouth and the seawater inflow through the bottom do not necessarily divide the water column evenly. Future improvements could include allowing the two layers to have different thicknesses.

Furthermore, the morphodynamical evolution of the estuary bed depth over a centennial timescale, while potentially significant, has been neglected in this study. Incorporating a sediment module into the EBM to simulate mass changes in the bed sediments and translate them into depth changes would be an important but challenging enhancement. In this study, a fully-physics-based EBM is used with coefficients calibrated for the Po di Goro branch as in Verri et al. (2021). We are planning to employ advanced machine learning and deep learning techniques to make the EBM outcomes even more accurate and easily relocatable (Saccotelli et al., 2024; Maglietta et al., 2024).

2.2.2 The set of experiments

We carried out three experiments from 1991 to 2100 by using the EBM and the available Regional Climate Models (RCMs) for the climate scenario RCP 8.5 to provide the necessary hydrology and marine forcings across historical and future climate periods. The RCP 8.5 emission scenario, considered here, follows the IPCC "business as usual" pathway, which assumes the GHG emission will continue to rise without mitigation policy, leading to radiative forcing exceeding 8.5 W/m^2 by 2100. The boundary fields entering the EBM experiments are as follows:

- River inflow at the estuary head (Figure 3, top panel). The yearly mean river discharge consists of
  (i) observed runoff from 1991 to 2005, based on *in situ* records

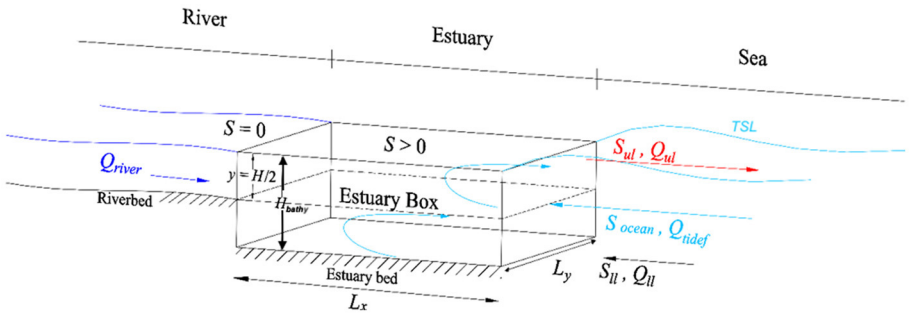

FIGURE 2
Sketch of the EBM model. Black, blue, and light blue arrows stand for the input variables coming from coupled models or observational datasets: Q_{river} is the inflowing river volume flux, Q_{tide_f} and Q_{ll} are the baroclinic and barotropic inflowing volume flux from the ocean, and S_{ll} and S_{ocean} are the inflowing salinity. Red arrows indicate the unknowns solved by the EBM: Q_{ul} is the estuarine outflowing volume flux and S_{ul} is the outflowing salinity. L_x is the length of salt-wedge intrusion.The pairs of curved arrows represent the inner tidal mixing.

at the Pontelagoscuro station, located upstream of the Po Delta, ~80 km inland from the river mouths (Arpae operative monitoring system https://simc.arpae.it/dext3r/),
(ii) projected runoff at the Pontelagoscuro station, derived from a coupled atmosphere-hydrology RCM (Vezzoli et al., 2015) from the EURO-CORDEX framework at ~8 km horizontal resolution, under the RCP 8.5 emission scenario, for the period 2006 to 2100. The 13% of the runoff values referring to the Pontelagoscuro station was extracted to be representative of the runoff entering the Po Goro branch, based on the partitioning provided by Arpae monitoring campaigns.

- Ocean inflow at the estuary mouth. The total sea level (TSL) (Figure 3, middle panel), the inland baroclinic velocity, and the inflowing sea salinity (ISS) (Figure 3, bottom panel) are derived from a coupled atmosphere-ocean Regional Climate Model within the MedCordex framework. The ocean component in this framework operates at ~12 km grid spacing (Cavicchia et al., 2018). This RCM runs in historical mode till 2005 and in projection mode under RCP 8.5 from 2006 onward. A correction methodology, detailed in the Appendix A, is applied to adjust the TSL trend at the river mouth. The barotropic tidal velocity at the river mouth is taken from the OTPS barotropic model (Egbert and Erofeeva, 2002).

Numerical experiments 1 and 2 employ a mechanistic approach to address key questions on the combined effects contributing to SWI changes:

- Experiment 1: full forcing experiment. The EBM has a variable water level $H_{tot}(t) = |H_{bathy}| + TSL(t)$. This means the TSL for the ellipsoid of reference is added to the river mouth depth H_{bathy}. This experiment aims to answer the question: are the SWI and the outflowing salinity at the river mouth changing in the future climate?
- Experiment 2: no sea level rise experiment. This is similar to Experiment1, but with the constant estuary depth at the river mouth, i.e., $H_{tot}(t) = |H_{bathy}|$. This experiment aims to answer the question: what is the relative role of the SLR on the Po di Goro estuarine dynamics?

Finally, a third experiment is a Digital Twin to Exp. 1 for assessing NBS in terms of the reduction of ISS:

- Experiment 3: Digital Twin for NBS. Similar to Experiment 1, but with a hypothesis asserting that 20% of the estuary water volume is covered with the halophytes along the estuary banks, thus reducing the salt of the inflowing seawater according to the empirical law proposed in Equation 11 in Appendix B. This means that S_{ocean} and S_{ll} entering Equations 2–4 read as below:

$$S_{ll_{exp3}} = 80\%S_{ll} + 20\%S_{ll_{residual}} \quad (5)$$

$$S_{ocean_{exp3}} = 80\%S_{ocean} + 20\%S_{ocean_{residual}} \quad (6)$$

where $S_{ll_{residual}}$ and $S_{ocean_{residual}}$ are computed following the empirical relationship in Equation 12 in Appendix B.

This Exp aims to answer the following question: what is the effect of a site-specific NBS on the increasing SWI of the Po di Goro estuary?

The characteristics of the experiments are summarized in Table 1.

3 Analysis of results

Four climate windows are considered for the analysis of the results of the Experiments: the historical time slice from 1991 to 2020, the short-term future covering 2021 to 2050, the mid-term future slice from 2051 to 2080, and the long-term future slice from 2081 to 2100.

The main drivers of the estuarine dynamics are shown in Figure 3, analyzed in the four climate windows. River discharge exhibits a negative trend in all windows, with the greatest decrease occurring in the mid-term 2051–2080. The TSL shows a positive trend with the largest increase in the long term 2081–2100. According to the RCM projection, the ISS is found

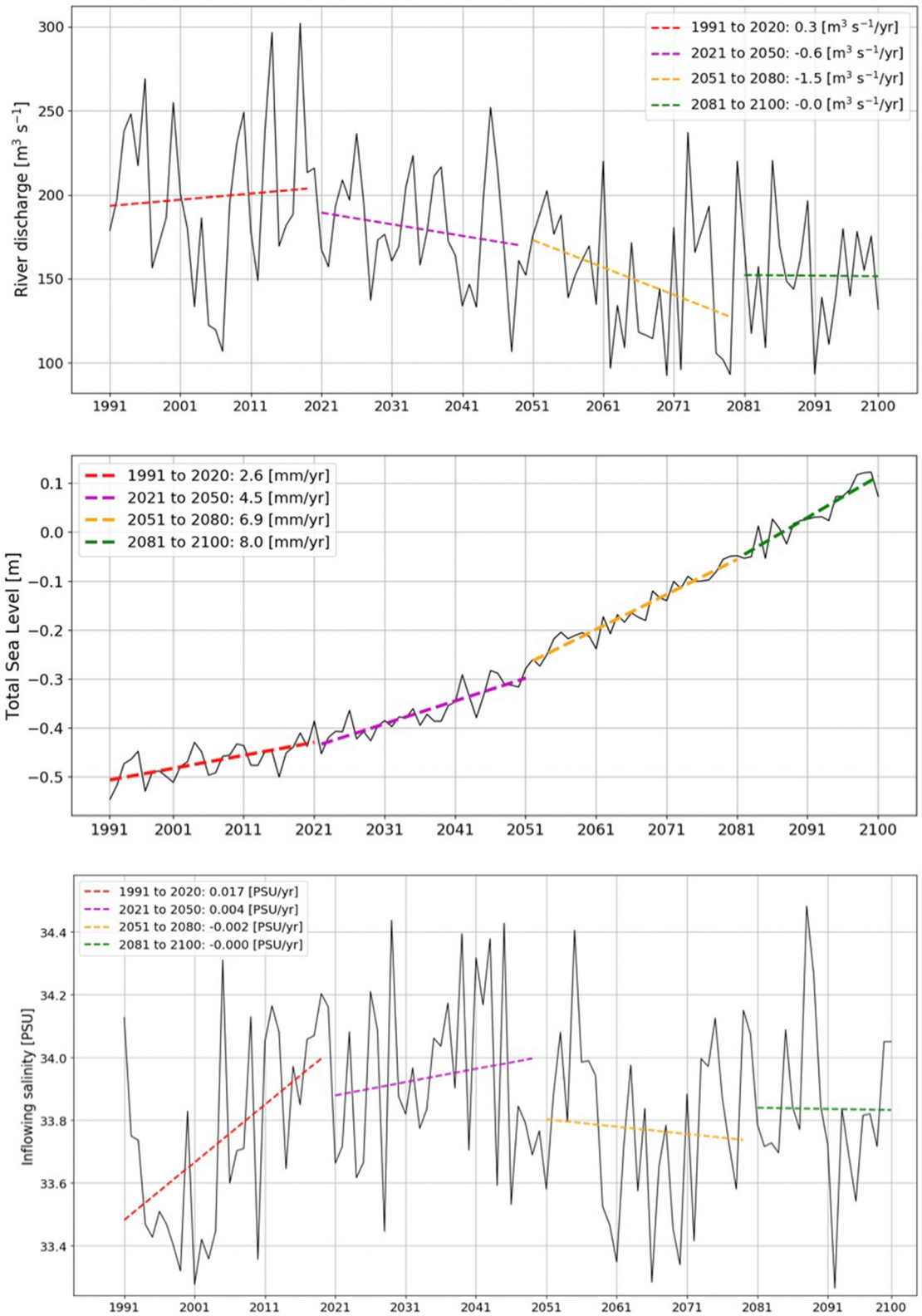

FIGURE 3
Timeseries of the yearly mean Po Goro river discharge at the estuary head **(top panel)**, the yearly mean total sea level TSL **(middle panel)**, and the yearly mean inflowing sea salinity ISS **(bottom panel)** at the estuary mouth over the whole climate range 1991–2100 for the scenario RCP 8.5. The linear trends are shown for the selected climate windows.

TABLE 1 Numerical experiments and their input conditions.

Numerical experiment	Climate range	River inflow at estuary head discharge (m^3/s)	Inflow at river mouth		
			Discharge (m^3/s)	Salinity (psu)	Total sea level TSL (m)
Experiment 1	1991–2005	Observations	RCM historical	RCM historical	RCM historical
	2006–2100	RCM RCP 8.5	RCM RCP 8.5	RCM RCP 8.5	RCM RCP 8.5 + correction
Experiment 2	1991–2005	Observations	RCM historical	RCM historical	Null
	2006–2100	RCM RCP8.5	RCM RCP 8.5	Projection	Null
Experiment 3	1991–2005	Observations	RCM historical	RCM historical reduced by NBS retention	RCM historical + correction
	2006–2100	RCM RCP 8.5	RCM RCP 8.5	RCM RCP 8.5 reduced by NBS retention	Projection + correction

to maintain a positive trend in the short-term future and stabilize in the long term. There is no observable trend in the baroclinic velocity of the inflowing seawater through the bottom (not shown).

3.1 Are the SWI and the outflowing salinity at the river mouth changing in the future climate?

Figures 4, 5 show the SWI and the outflowing salinity for the average day-of-year in Exp. 1 across the three periods. In all time slices, the Po di Goro estuary experiences an increase in SWI length and river mouth salinity, compared to the present state. The highest increase occurs in summer when the river discharge is lowest as shown in Figure 6.

As summarized in Tables 2–5, the Experiment 1 shows:

- SWI length will increase by +43% (63%) in mid-term (long term) on annual basis and with the highest increase of +79% (+120%) in summer;
- Estuarine outflowing salinity will increase of +18% (26.7%) in mid-term (long term) on annual basis compared to the historical range and with the peak values of +51% (+69%) in summer.

The mid-term period shows the highest growth rate for both SWI length and river mouth salinity, coinciding with the largest decrease in river discharge, i.e., $-1.5m^3s^{-1}/yr$ (Figure 3 top panel). In the long-term future, when the river discharge reaches its lowest values with a null trend (Figure 3 top panel), the increase for both SWI length and outflowing salinity hint that the trends are still positive but lower than short and mid-terms.

Finally, the river mouth salinity slightly reduces on winter and spring through all future slices, especially in the long-term one. This can be explained with the higher discharge during these seasons in the long-term slice (see Figure 6), likely due to the positive trend in winter precipitation, leading to a higher frequency of high-flow events, and the earlier onset of snow-melting in the Po catchment compared to the historical norms (Coppola et al., 2014).

The right panels of Figures 4, 5 provide the probability density function (PDF) for the SWI and the outflowing salinity, respectively. They have been obtained using the Kernel Density Estimation (KDE) non-parametric method. In our analysis, KDE is generated based on a Gaussian kernel. Bandwidths were determined by Scott's rule for the unimodal SWI length distribution and a manual selector for the multimodal outflowing salinity distribution.

The right panels of Figure 4 indicate that the SWI PDF is becoming more skewed and heavy-tailed in the mid- and long-term future. The most probable value of $8km$ remains consistent across time slices, but the probability reduces by one-third (half) in the mind-(long-) term future. The kurtosis coefficient becomes negative in the long term meaning that the PDF with heavy right tail is moving toward a bimodal distribution with a second local maximum at around 20km.

Similarly, the outflowing salinity PDFs in the right-hand panels of Figure 5 show increased skewness and heavier tails in the mid- and long term compared to the historical range. In the long term, the salinity distribution evolves from bimodal to trimodal, with a new local maximum at ∼30 km.

The overall conclusion from the PDF analysis presented in the right panels of Figures 4, 5 is that the estuarine dynamics regime is shifting toward a more complex multimodal distribution when transitioning from historical to long-term future conditions. In this shift, outliers representing extreme values of the SWI length and the outflowing salinity in the historical PDFs become significantly more frequent in the projected PDFs, indicating potential shifts to alternative stable states in the future.

3.2 What is the relative role of the SLR and the RDD in Po di Goro estuarine dynamics?

To address this question, we compare the SWI and the outflowing salinity for Experiments 1 and 2 (Figures 4, 5). The SLR contributes to increase the SWI length and the estuary outflowing salinity. Increasing the total sea level at the estuary mouth means lower internal Froude number

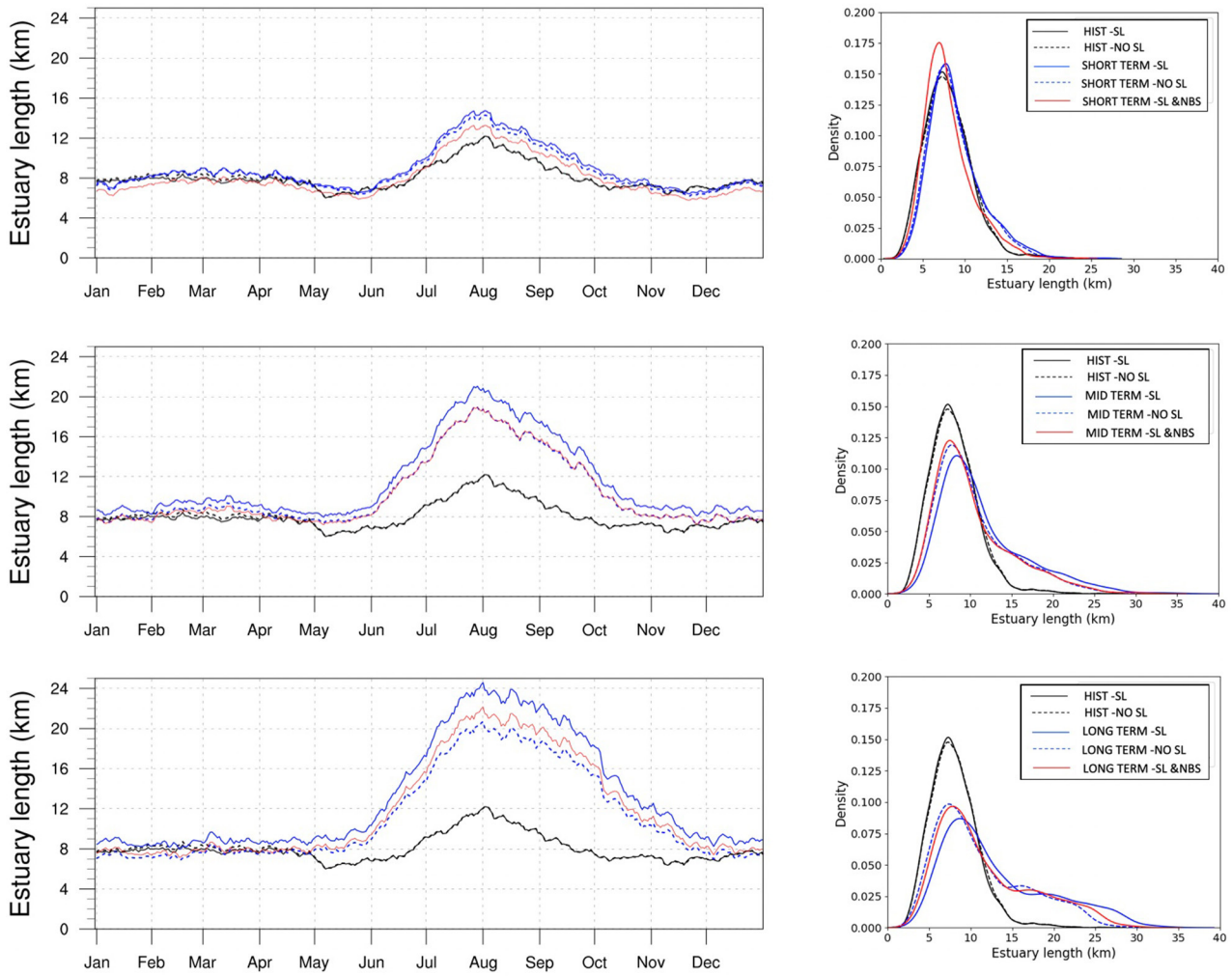

FIGURE 4
SWI length: the average day-of-year **(left)** and the probability density function **(right)**. Top, middle, and bottom panels refer to short-term, mid-term, and long-term ranges. Black lines refer to the historical range, with (firm line, Experiment 1) and without (dashed line, Experiment 2) SL. Blue lines refer to the future range, with (firm line, Experiment 1) and without (dashed line, Experiment 2) SL. Red line refers to the future range with SL and NBS (Experiment 3).

$Fr_{estuary}$ and higher gradient Richardson number $Ri_{estuary}$ (Geyer and Smith, 1987). In the EBM, these are defined as follows:

$$Fr_{estuary} = \frac{{u_{ul}}^2}{gH_{tot}} \tag{7}$$

$$Ri_{estuary} = \frac{\frac{g}{\rho_0}\frac{d\rho}{dz}}{(\frac{du}{dz})^2} = \frac{gk_s\frac{S_{ll}-S_{ul}}{H_{tot}/2}}{\left(\frac{u_{ll}+u_{tide_f}-u_{ul}}{H_{tot}/2}\right)^2} \tag{8}$$

The estuarine water column is thus more marine-dominated (lower $Fr_{estuary}$) and higher stratified (higher $Ri_{estuary}$) when the SLR becomes significant, allowing the salt wedge to progress further inland. The gradient Richardson number is an effective dimensionless metric for assessing estuarine dynamics and the resulting salt-wedge intrusion. It depends on the density (salinity) gradient and the squared velocity gradient: positive (negative) values mean stratified (mixed) system. However, positive values below 0.25 (the threshold for dynamic instability) suggest unstable stratification due to velocity shear.

The potential SLR impact is site-specific and depends on the estuary geometry, the tidal range, and the discharge regime. The SLR impacts are more (less) pronounced in shallow (deep) estuaries, micro (macro) tidal environment, and low (high) river discharge regime (Krvavica and Ružić, 2020; Prandle and Lane, 2015). The Po di Goro branch flows into a micro-tidal sea but it has a river-dominated estuary and the river mouth depth is one order of magnitude higher than the local sea level fluctuations. Another clear result is that the increasing SWI length and the river mouth salinity exhibit a non-linear response to the river discharge and the TSL. River discharge supports vertical mixing inside the estuary, while the TSL promotes the estuary stratification. In a river-dominated estuary such as Po di Goro one, river

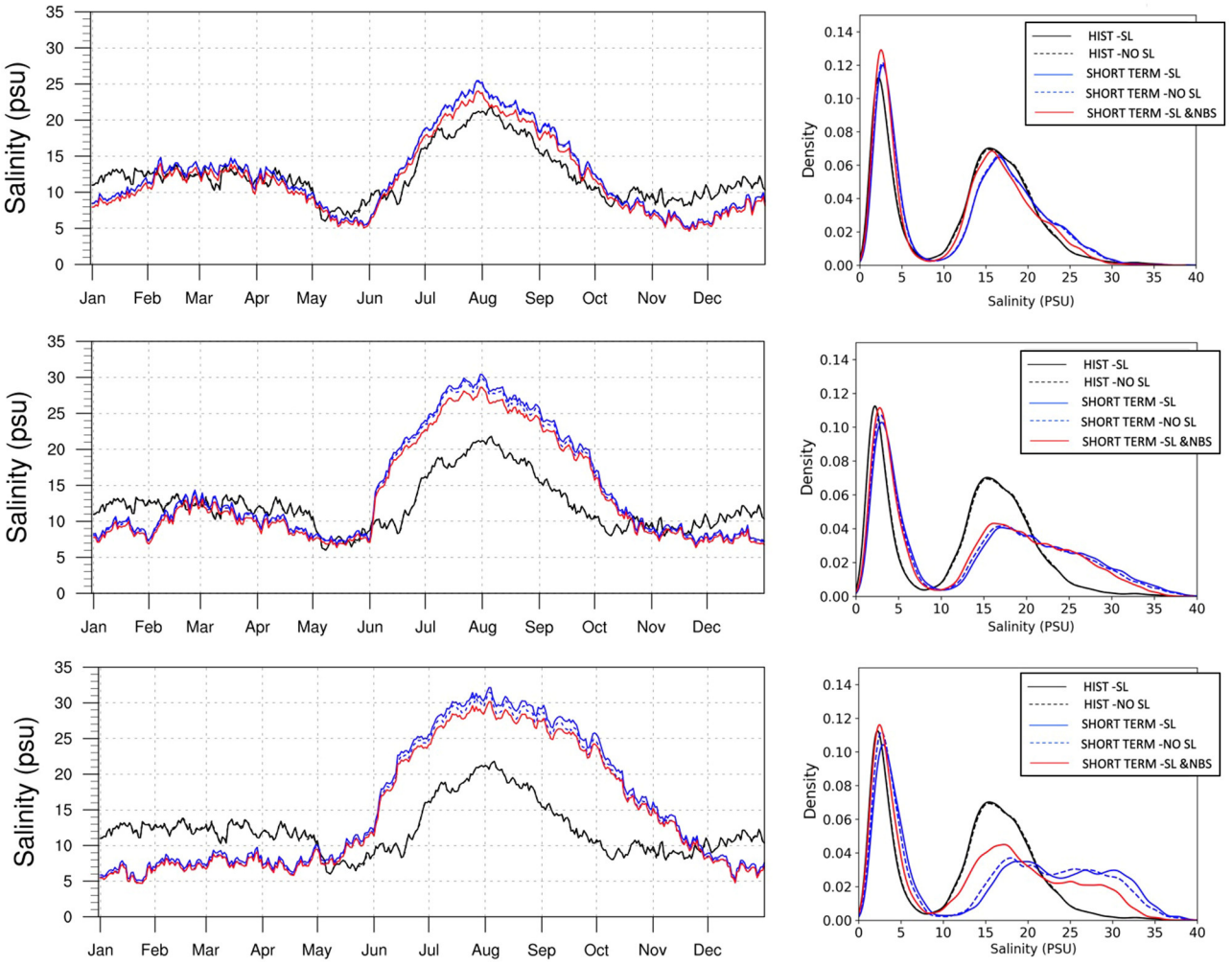

FIGURE 5
River mouth outflowing salinity: the average day-of-year **(left)** and the probability density function **(right)**. Top, middle, and bottom panels refer to short-term, mid-term, and long-term ranges. Black lines refer to the historical range, with (firm line, Experiment 1) and without (dashed line, Experiment 2) SL. Blue lines refer to the future range, with (firm line, Experiment 1) and without (dashed line, Experiment 2) SL. Red line refers to the future range with SL and NBS (Experiment 3).

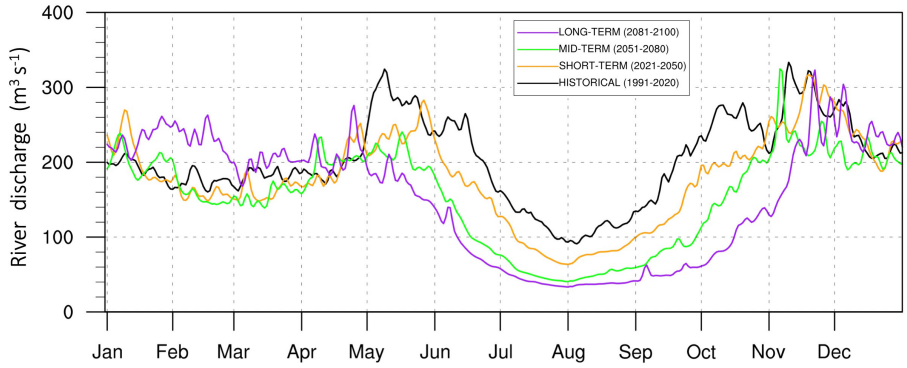

FIGURE 6
Average day-of-year of river discharge. Black, yellow, green, and violet lines refer to the historical, short-term, mid-term, and long-term window, respectively.

10.3389/fclim.2024.1408038

TABLE 2 Yearly averaged SWI length.

Year	AVG (km)			Increase/decrease (%) (future vs. historical)		
Historical 1991–2020	8.02	8.10	/	/	/	/
Short term 2021–2050	8.90	8.68	8.02	+11	+8.3	+0.01
Mid-term 2051–2080	11.45	10.38	10.31	+42.7	+29.4	+28.6
Long term 2081–2100	13.10	11.15	11.79	+63.4	+39.1	+47.0
	Exp1	Exp2	Exp3	Exp1	Exp2	Exp3

TABLE 3 Seasonal averaged SWI length.

Winter	AVG (km)			Increase/decrease (%) (future vs historical)		
Historical 1991–2020	7.84	8.09	/	/	/	/
Short term 2021–2050	8.25	8.22	7.42	+5.3	+4.9	−5.3
Mid-term 2051–2080	9.13	8.42	8.21	+16.5	+7.7	+4.8
Long term 2081–2100	8.67	7.48	7.77	+10.6	−4.6	−0.8
	Exp1	Exp2	Exp3	Exp1	Exp2	Exp3
Spring	**AVG (km)**			**Increase/decrease (%) (future vs historical)**		
Historical 1991–2020	7.24	7.32	/	/	/	/
Short term 2021–2050	7.80	7.65	7.06	+7.7	+5.5	−2.6
Mid-term 2051–2080	9.74	8.95	8.82	+34.5	+23.5	+21.8
Long term 2081–2100	10.77	9.33	9.74	+48.6	+28.8	+34.4
	Exp1	Exp2	Exp3	Exp1	Exp2	Exp3
Summer	**AVG (km)**			**Increase/decrease (%) (future vs. historical)**		
Historical 1991+-2020	9.86	9.86	/	/	/	/
Short term 2021–2050	12.15	11.73	10.95	+23.3	+19.1	+11.1
Mid-term 2051–2080	17.65	15.83	15.89	+79	+60.6	+61.3
Long term 2081–2100	21.71	18.29	19.53	+120.3	+85.6	+98.2
	Exp1	Exp2	Exp3	Exp1	Exp2	Exp3
Autumn	**AVG (km)**			**Increase/decrease (%) (future vs historical)**		
Historical 1991–2020	7.13	7.13	/	/	/	/
Short term 2021–2050	7.38	7.12	6.64	+3.4	−0.2	−7.0
Mid-term 2051–2080	9.19	8.25	8.26	+28.8	+15.6	+15.8
Long term 2081–2100	11.15	9.41	10.01	+56.3	+31.9	+40.3
	Exp1	Exp2	Exp3	Exp1	Exp2	Exp3

TABLE 4 Yearly averaged outflowing salinity.

Year	AVG (psu)			Increase/decrease (%) (future vs historical)		
Historical 1991–2020	12.28	12.30	/	/	/	/
Short term 2021–2050	12.56	12.49	11.83	+2.2	+1.6	−3.7
Mid-term 2051–2080	14.50	14.16	13.63	+18	+15.2	+11
Long term 2081–2100	15.56	15.03	14.63	+26.7	+22.3	+19.1
	Exp1	Exp2	Exp3	Exp1	Exp2	Exp3

TABLE 5 Seasonal averaged outflowing salinity.

Winter	AVG (psu)			Increase/decrease (%) (future vs historical)		
Historical 1991–2020	12.30	12.43	/	/	/	/
Short term 2021–2050	12.06	12.06	11.35	−2.0	−1.9	−7.7
Mid-term 2051–2080	10.75	10.49	10.08	−12.6	−14.7	−18.1
Long term 2081–2100	7.45	7.10	6.95	−39.4	−42.3	−43.5
	Exp1	Exp2	Exp3	Exp1	Exp2	Exp3
Spring	**AVG (psu)**			**Increase/decrease (%) (future vs historical)**		
Historical 1991–2020	10.06	10.03	/	/	/	/
Short term 2021–2050	10.23	10.19	9.65	+1.7	+1.2	−4.1
Mid-term 2051–2080	12.08	11.83	11.39	+20.1	+17.6	+13.2
Long term 2081–2100	13.05	12.64	12.31	+29.7	+25.6	+22.3
	Exp1	Exp2	Exp3	Exp1	Exp2	Exp3
Summer	**AVG (psu)**			**Increase/decrease (%) (future vs historical)**		
Historical 1991–2020	16.96	16.97	/	/	/	/
Short term 2021–2050	20.13	19.95	18.98	+18.7	+17.6	+11.9
Mid-term 2051–2080	25.6	25.1	24.1	+50.9	+47.8	+42
Long term 2081–2100	28.69	27.87	26.97	+69.1	+64.3	+59.0
	Exp1	Exp2	Exp3	Exp1	Exp2	Exp3
Autumn	**AVG (psu)**			**Increase/decrease (%) (future vs historical)**		
Historical 1991–2020	9.79	9.75	/	/	/	/
Short term 2021–2050	7.78	7.70	7.30	−20.5	−21.3	−25.4
Mid-term 2051–2080	9.45	9.14	8.86	−3.5	−6.6	−9.5
Long term 2081–2100	12.86	12.30	12.10	+31.4	+25.7	+23.6
	Exp1	Exp2	Exp3	Exp1	Exp2	Exp3

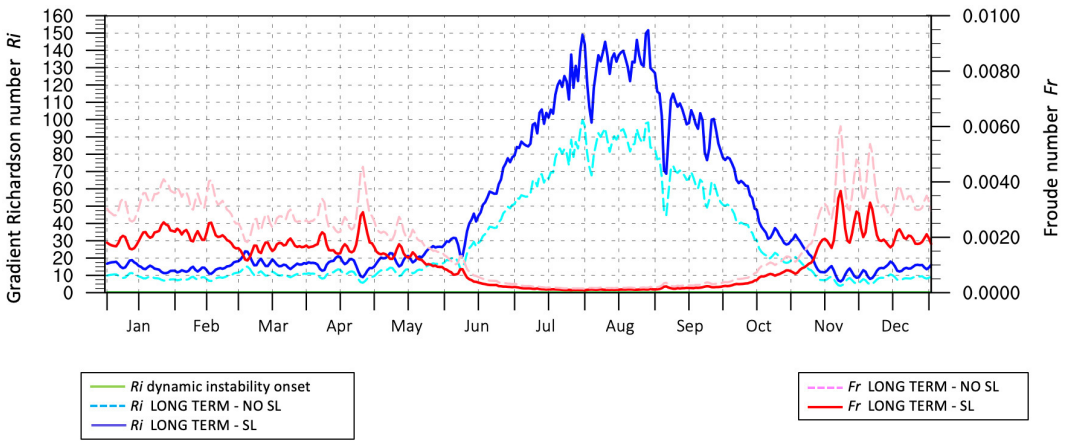

FIGURE 7
Gradient Richardson number *Ri* and Froude number *Fr* for the average day-of-year over 2081–2100. Firm blue and red lines refer to Experiment 1 with SL. Dashed cyan and pink lines refer to Experiment 2 without SL. The green line identifies the "dynamic instability onset" when Gradient Richardson number is 0.25.

discharge primarily drives estuary dynamics making RDD the main driver of salinization and increased SWI. SLR acts in the same direction as RDD, with the most pronounced effect in the long-term future when the RDD trend is null, as shown in the left bottom panel of Figure 4 with clearly detached firm and dashed blue lines.

We argue that this interpretation is supported by the timeseries of the internal Froude number and the gradient Richardson

number shown in Figure 7 for both Experiments 1 and 2. *Ri* is higher, and *Fr* is lower in Experiment 1 than Experiment 2. The greatest differences can be seen in the long term, where SLR promotes conditions favorable for SWI. SLR also has a weaker but discernible effect on estuary outflowing salinity, as indicated by the slightly separated solid and dashed blue lines in the left bottom panel of Figure 5. The Experiment 2 results can be summarized as shown in Tables 2–5:

- SWI length will increase of +29% (39%) in mid-term (long term) on annual basis and with the highest percentages +61% (+86%) in summer. It is worth noting that the summer increase percentage of 86% in the long-term future is close to the increase percentage of 81%found by Bellafiore et al. (2021). With respect to Experiment 1, the Exp. 2 results mean that the change in the river flow is the main driver of Po di Goro SWI for both time slices. However, the SLR plays an important role on SWI and becomes more relevant in the summer time and in the long-term slice i.e., when the river flow reduces to lowest values: in the mid-term, the SLR is responsible for 13% on annual basis and up to 18% in summer time, and in the long term the SLR role rises to 24% on annual basis and till 34% in summer time.
- River mouth salinity will increase of +15% (22%) in mid-term (long term) on annual basis and with the peak values of +48% (+64%) in summer. With respect to Experiment 1, this means that the change in the river flow is the main mechanism regulating the Po di Goro estuary outflowing salinity and the SLR plays a minor role. Its effect on the increasing river mouth salinity reaches 4.4% on annual basis (4.8% in summer time) in the long term.

The probability density functions (PDFs) in Figures 4, 5 indicate that the SLR plays a minor role in the Po di Goro river SWI and salinity runoff. Its main effect is on altering extreme events in the long-term future.

3.3 What is the potential effect of a site-specific NBS on the increasing SWI of the Po di Goro estuary?

The mitigation effect of the Atriplex portulacoides on the potential increase in (i) river mouth salinity and (ii) SWI length was demonstrated by investigating several halophyte species (Appendix B).

The Digital Twin Experiment 3 assumes that the halophytes selected as site-specific NBS interact with 20% of the total estuary water volume. This then reduces the salt of the inflowing seawater according to the empirical law proposed in Equation 12 in Appendix B, thus with the EBM inflowing salinity fields given by the new Equations 5, 6.

The red lines in the panels of Figures 4, 5 show how the NBS reduces both the SWI and the outflowing salinity. The positive effect is larger in summer time and reaches the maximum effect in the long-term future.

Overall, the proposed NBS shows an "retarding effect" on salinization which may also be viewed as a "restoring effect" if actions are taken in the short-term future when they are demonstrated to ensure 0% increase of salt-wedge intrusion (Table 2 and top panel of Figure 4) and −4% change of the river mouth salinity (Table 4 and top panel of Figure 5) with respect to the historical range.

The present study does not adequately consider the ISS at the river mouth. In fact the RCM does not show a significant increase of ISS, i.e., the ISS averaged over the long-term window is only 0.1 psu higher than the one over the historical window. More recent and high-resolution climate projections for the Adriatic sea indicate a much stronger increase of the sea surface salinity in the coastal areas on the western side of the Adriatic basin. In addition, the higher the ISS, the higher the salt uptake of the halophytes (see Equation 12 in Appendix B). For all these reasons, we argue that the potential effect of the specific NBS here proposed is underestimated.

The results of Experiment 3 can be summarized as follows (see Tables 2–5):

- SWI length is predicted to increase b+0.01% in short term, +28.6% in mid-term, and +47% in long term on annual basis and with the highest percentages (+11%, +61%, and +98% in short, middle, and long term) in summer. With respect to Experiment 1, this means the proposed NBS counteracts the increase of SWI: the reduction of SWI by the NBS on annual (summer) basis is 14% (18%) in the mid-term and 16% (22%) in the long term.
- River mouth salinity will vary of −3% in short term, +11% in mid-term, and 19% in long term on annual basis. The highest percentages (+12%, +42%, and +59% in short, middle, and long term) are in summer. With respect to Experiment 1, this means the proposed NBS slightly counteracts the increase of estuary outflowing salinity

By comparing the PDF red and blue lines in Figure 4, we can argue that the NBS moves the peak and the tail of the SWI distribution leftward and slightly increases the new leftward peak values. On the short term slice, the peak value of the red line is even higher than the one of the historical distribution (black line), and the skewness is less marked. Regarding the distribution of the river mouth salinity (Figure 5), the main effect is in the long-term time slice distribution.

4 Conclusion

This study has examined the compound effect of SLR and RDD on a salt-wedge estuary under changing climate using climate projections. Additionally, we formulated a Digital Twin experiment to assess the potential of applying a site-specific NBS. An intermediate-complexity estuary model, the CMCC EBM, was employed, and climate projection simulations were conducted.

A set of three centennial climate experiments covering 1991–2100 was proposed over the Po di Goro estuary, two using a mechanistic approach and the third representing a Digital Twin experiment to assess local NBS. The results show that the increasing SWI in the Po di Goro estuary under changing climate is a non-linear response to the RDD in first instance and the SLR. The

discharge decrease acts as the main driver and shows a large negative trend till mid-term future (i.e., 2050–2080) while the SLR becomes significant in the long-term future (i.e., 2080–2100) as the RDD trend stabilizes. The SWI increase is largest in the summer time; the outflowing river salinity increases across all time slices, especially in summer.

The salt retention capability of the Atriplex portulacoides in the estuaries estuaries represents a promising adaptation strategy to counteract inland water salinization, particularly in the mid-term (2050–2080). The Digital Twin experiment carried out warrants deeper investigations, for example, with changing distributions of the NBS.

Finally, future analyses will leverage higher-resolution coastal Earth system climate downscaling, such as that developed in the AdriaCLIM project (Verri et al., 2024) to provide more accurate and localized estimates of river runoff, sea surface height, and currents. Additionally, a more efficient EBM, integrating machine learning and deep learning techniques (Saccotelli et al., 2024; Maglietta et al., 2024) will be tested for centennial-scale simulations. Plans are also underway to include the morphodynamical evolution of the estuary bed.

Data availability statement

The physically based EBM here used for performing the experiments is freely downloadable from its webpage https://www.estuaryboxmodel.org. Further inquiries can be directed to the corresponding author.

Author contributions

GV: Conceptualization, Formal analysis, Investigation, Methodology, Software, Supervision, Visualization, Writing – original draft, Writing – review & editing. AD: Data curation, Investigation, Validation, Visualization, Writing – review & editing. VS: Data curation, Visualization, Writing – review & editing. AS: Data curation, Methodology, Writing – review & editing. AL: Data curation, Methodology, Writing – review & editing. MR: Data curation, Investigation, Writing – review & editing. EM: Data curation, Investigation, Writing – review & editing. SD: Data curation, Investigation, Writing – review & editing. GC: Funding acquisition, Supervision, Writing – review & editing. NP: Funding acquisition, Methodology, Supervision, Writing – review & editing.

Funding

The author(s) declare financial support was received for the research, authorship, and/or publication of this article. This research was funded by the OPERANDUM project of the European Union's Horizon 2020 research and innovation program under grant agreement no. 776848. Partial financial support came from the AdriaClim project (Climate change information, monitoring and management tools for adaptation strategies in Adriatic coastal areas; project ID 10252001) and from the Spoke 4 – ICSC–Centro Nazionale di Ricerca in High Performance Computing, Big Data and Quantum Computing, funded by European Union–NextGenerationEU; Project Name: PNRR-HPC; Project Number: CN00000013; CUP: C83C22000560007.

Acknowledgments

The authors are grateful to the Operandum project Coordinator, Prof. Silvana Di Sabatino, who strongly supported this study. The authors also thank the AdriaClim project Coordinator Dr. Andrea Valentini and the leading Partner Agency for Prevention, Environment and Energy of Emilia-Romagna (Arpae).

Conflict of interest

The authors declare that the research was conducted in the absence of any commercial or financial relationships that could be construed as a potential conflict of interest.

Publisher's note

References

Abbas, A. M., Figueroa, E., de Cires, A., Rubio-Casal, A. E., and Castillo, J. M. (2014). Effects of competition from the invasive cordgrass spartina densiflora on native atriplex portulacoides. *Int. J. Sci. Eng. Res.* 5, 209–212.

Ablain, M., Meyssignac, B., Zawadzki, L., Jugier, R., Ribes, A., Spada, G., et al. (2019). Uncertainty in satellite estimates of global mean sea-level changes, trend and acceleration. *Earth Syst. Sci. Data* 11, 1189–1202. doi: 10.5194/essd-11-1189-2019

Adloff, F., Jordà, G., Somot, S., Sevault, F., Arsouze, T., Meyssignac, B., et al. (2018). Improving sea level simulation in Mediterranean regional climate models. *Clim. Dyn.* 51, 1167–1178. doi: 10.1007/s00382-017-3842-3

Barenblatt, G. I. (1987). *Dimensional Analysis*. Boca Raton, FL: CRC Press.

Bellafiore, D., Ferrarin, C., Maicu, F., Manfè, G., Lorenzetti, G., Umgiesser, G., et al. (2021). Saltwater intrusion in a Mediterranean delta under a changing climate. *J. Geophys. Res. Oceans* 126:e2020JC016437. doi: 10.1029/2020JC016437

Borile, F., Pinardi, N., Lyubartsev, V., and Oddo, P. (2024). Mediterranean sea mean sea level slowdown: the effects of the water budget. *Front. Clim.*

Carafa, R., Marinov, D., Dueri, S., Wollgast, J., Ligthart, J., Canuti, E., et al. (2006). A 3D hydrodynamic fate and transport model for herbicides in Sacca di Goro coastal lagoon (Northern Adriatic). *Mar. Pollut. Bull.* 52, 1231–1248. doi: 10.1016/j.marpolbul.2006.02.025

Cavicchia, L., Scoccimarro, E., Gualdi, S., Marson, P., Ahrens, B., Berthou, S., et al. (2018). Mediterranean extreme precipitation: a multi-model assessment. *Clim. Dyn.* 51, 901–913. doi: 10.1007/s00382-016-3245-x

Cohen-Schacham, E., Walters, G., Janzen, C., and Maginnis, S. (2016). *Nature-based Solutions to Address Global Societal Challenges*. Gland: IUCN, 91–97. doi: 10.2305/IUCN.CH.2016.13.en

Colombani, N., Osti, A., Volta, G., and Matrocicco, M. (2016). Impact of climate change on salinization of coastal water resources. *Water Resour. Manag.* 30, 2483–2496. doi: 10.1007/s11269-016-1292-z

Coppola, E., Verdecchia, M., Giorgi, F., Colaiuda, V., Tomassetti, B., Lombardi, A., et al. (2014). Changing hydrological conditions in the Po basin under global warming. *Sci. Total Environ.* 493, 1183–1196. doi: 10.1016/j.scitotenv.2014.03.003

Corbau, C., Simeoni, U., Zoccarato, C., Mantovani, G., and Teatini, P. (2019). Coupling and use evolution and subsidence in the Po Delta, Italy: revising the past occurrence and prospecting the future management challenges. *Sci. Total Environ.* 654, 196–1208. doi: 10.1016/j.scitotenv.2018.11.104

Denamiel, C., and Vilibić, I. (2023). Next generation atmosphere-ocean climate modelling for storm surge hazard projections. *EGUsphere* 1–30. doi: 10.5194/egusphere-2023-913

Drenkard, E. J., Stock, C., Ross, A. C., Dixon, K. W., Adcroft, A., Alexander, M., et al. (2021). Next-generation regional ocean projections for living marine resource management in a changing climate. *ICES J. Mar. Sci.* 78, 1969–1987. doi: 10.1093/icesjms/fsab100

Egbert, G. D., and Erofeeva, S. Y. (2002). Efficient inverse modeling of Barotropic Ocean tides. *J. Atmos. Ocean. Technol.* 19, 183–204. doi: 10.1175/1520-0426(2002)019<0183:EIMOBO>2.0.CO;2

Galassi, G., and Spada, G. (2014). Sea-level rise in the Mediterranean sea by 2050: Roles of terrestrial ice melt, steric effects and glacial isostatic adjustment. *Glob. Planet. Change* 123, 55–66. doi: 10.1016/j.gloplacha.2014.10.007

Gallotti, G. A., S. M., Apostolidou, I., Di Sabatino, S. (2021). On the management of nature-based solutions in open-air laboratories: new insights and future perspectives. *Resources* 10:36. doi: 10.3390/resources10040036

Geyer, W. R., and MacCready, P. (2014). The estuarine circulation. *Annu. Rev. Fluid Mech.* 46, 175–197. doi: 10.1146/annurev-fluid-010313-141302

Geyer, W. R., and Smith, J. D. (1987). Shear instability in a highly stratified estuary. *J. Phys. Oceanogr.* 17, 1668–1679. doi: 10.1175/1520-0485(1987)017<1668:SIIAHS>2.0.CO;2

Holt, J., Harle, J., Wakelin, S., Jardine, J., and Hopkins, J. (2022). Why is seasonal density stratification in shelf seas expected to increase under future climate change? *Geophys. Res. Lett.* 49:e2022GL100448. doi: 10.1029/2022GL100448

Holt, J., Hyder, P., Ashworth, M., Harle, J., Hewitt, H. T., Liu, H., et al. (2017). Prospects for improving the representation of coastal and shelf seas in global ocean models. *Geosci. Model Dev.* 10, 499–523. doi: 10.5194/gmd-10-499-2017

Koirala, S., Hirabayashi, Y., Mahendran, R., and Kanae, S. (2014). Global assessment of agreement among streamflow projections using CMIP5 model outputs. *Environ. Res. Lett.* 9:064017. doi: 10.1088/1748-9326/9/6/064017

Krvavica, N., and Ružić, I. (2020). Assessment of sea-level rise impacts on salt-wedge intrusion in idealized and Neretva River Estuary. *Estuar. Coast. Shelf Sci.* 234:106638. doi: 10.1016/j.ecss.2020.106638

Kurdistani, S., Verri, G., Pinardi, N., and Coppini, G. (2022). *Climate Projections of salt-wedge intrusions in a Po river branch (Northern Adriatic Sea).*

Kurdistani, S. M., Tomasicchio, G. R., D'Alessandro, F., and Hassanabadi, L. (2019). River bank protection from ship-induced waves and river flow. *Water Sci. Eng.* 12, 129–135. doi: 10.1016/j.wse.2019.05.002

Lee, J., Biemond, B., de Swart, H., and Dijkstra, H. A. (2024). Increasing risks of extreme salt intrusion events across European estuaries in a warming climate. *Commun. Earth Environ.* 5. doi: 10.1038/s43247-024-01225-w

Little, S., Wood, P. J., and Elliott, M. (2016). Quantifying salinity-induced changes on estuarine benthic fauna: the potential implications of climate change. *Estuar. Coast. Shelf Sci.* 198, 610–625. doi: 10.1016/j.ecss.2016.07.020

Lorenz, M., Klingbeil, K., and Burchard, H. (2021). Impact of evaporation and precipitation on estuarine mixing. *J. Phys. Oceanogr.* 51, 1319–1333. doi: 10.1175/JPO-D-20-0158.1

MacCready, P. (2004). Toward a unified theory of tidally-averaged estuarine salinity structure. *Estuaries* 27, 561–570. doi: 10.1007/BF02907644

Maglietta, R., Verri, G., Saccotelli, L., De Lorenzis, A., Cherubini, C., Caccioppoli, R., et al. (2024). Advancing estuarine box modeling: a novel hybrid machine learning and physics-based approach. *Environ. Model. Softw.* doi: 10.1016/j.envsoft.2024.106223

Meli, M., Camargo, C. M. L., Olivieri, M., Slangen, A. B. A., and Romagnoli, C. (2023). Sea-level trend variability in the Mediterranean during the 1993–2019 period. *Front. Mar. Sci.* 11, 1189–1202. doi: 10.3389/fmars.2023.1150488

Neves, J. P., Ferreira, L. F., Simoes, M. P., and Gazarini, L. C. (2007). Primary production and nutrient content in two salt marsh species, *Atriplex portulacoides* l., *Limoniastrum monopetalum* l., in Southern Portugal. *Estuaries Coasts* 30, 459–468. doi: 10.1007/BF02819392

Pillai, U. P. A., Pinardi, N., Alessandri, J., Federico, I., Causio, S., Unguendoli, S., et al. (2022). A Digital Twin modelling framework for the assessment of seagrass Nature Based Solutions against storm surges. *Sci. Total Environ.* 847:157603. doi: 10.1016/j.scitotenv.2022.157603

Pinardi, N., Bonaduce, A., Navarra, A., Dobricic, S., and Oddo, P. (2014). The mean sea level equation and its application to the mediterranean sea. *J. Clim.* 27, 442–447. doi: 10.1175/JCLI-D-13-00139.1

Piña-Valdés, J., Socquet, A., Beauval, C., Doin, M. P., D'Agostino, N., Shen, Z. K. (2022). 3d gnss velocity field sheds light on the deformation mechanisms in Europe: effects of the vertical crustal motion on the distribution of seismicity. *J. Geophys. Res. Solid Earth* 127:e2021JB023451. doi: 10.1029/2021JB023451

Pörtner, H.-O., Roberts, D., Tignor, M., Poloczanska, E., Mintenbeck, K., Alegría, A., et al. (eds.) (2022). *IPCC, 2022: Climate Change 2022: Impacts, Adaptation, and Vulnerability. Contribution of Working Group ii to the Sixth Assessment Report of the Intergovernmental Panel on Climate Change*. Cambridge: Cambridge University Press, 3056.

Prandle, D., and Lane, A. (2015). Sensitivity of estuaries to sea level rise: vulnerability indices. *Estuar. Coast. Shelf Sci.* 160, 60–68. doi: 10.1016/j.ecss.2015.04.001

Saccotelli, L., Verri, G., De Lorenzis, A., Cherubini, C., Caccioppoli, R., Coppini, G., et al. (2024). Enhancing estuary salinity prediction: a Machine Learning and Deep Learning based approach. *Appl. Comput. Geosci.* 23:100173. doi: 10.1016/j.acags.2024.100173

Sannino, G., Carillo, A., Iacono, R., Napolitano, E., Palma, M., Pisacane, G., et al. (2022). Modelling present and future climate in the Mediterranean sea: a focus on sea-level change. *Clim. Dyn.* 59, 357–391. doi: 10.1007/s00382-021-06132-w

Storto, A., Bonaduce, A., Feng, X., and Yang, C. (2019). Steric sea level changes from ocean reanalyses at global and regional scales. *Water* 11. doi: 10.3390/w11101987

Tarolli, P., Luo, J., Straffelini, E., Liou, Y. A., Nguyen, K. A., Laurenti, R., et al. (2023). Saltwater intrusion and climate change impact on coastal agriculture. *PLoS Water* 2:e0000121. doi: 10.1371/journal.pwat.0000121

Tian, R. (2019). Factors controlling saltwater intrusion across multi-time scales in estuaries. *Estuar. Coast. Shelf Sci.* 223, 61–73. doi: 10.1016/j.ecss.2019.04.041

Tsz Yeung Leung, A., Stronach, J., and Matthieu, J. (2018). Modelling behaviour of the salt wedge in the Fraser river and its relationship with climate and man-made changes. *J. Mar. Sci. Eng.* 6:130. doi: 10.3390/jmse6040130

Valega, M., Lillebo, A. I., Caçador, I., Pereira, M. E., Duarte, A. C., Pardal, M. A., et al. (2008). Mercury mobility in a salt marsh colonised by Halimione portulacoides. *Chemosphere* 72, 1607–1613. doi: 10.1016/j.chemosphere.2008.04.007

Valle Levinson, A. (2010). *Contemporary Issues in Estuarine Physics, Definition and Classification of Estuaries*. Cambridge: Cambridge University Press. doi: 10.1017/CBO9780511676567

Verri, G., Barletta, I., Pinardi, N., Federico, I., Alessandri, J., Coppini, G., et al. (2023). Shelf slope, estuarine dynamics and river plumes in a z* vertical coordinate, unstructured grid model. *Ocean Model.* 184:102235. doi: 10.1016/j.ocemod.2023.102235

Verri, G., Furnari, L., Gunduz, M., Senatore, A., Santos da Costa, V., De Lorenzis, A., et al. (2024). Climate projections of the Adriatic Sea: the role of river release. *Front. Clim.* 6:1368413. doi: 10.3389/fclim.2024.1368413

Verri, G., Mahmoudi Kurdistani, S., Coppini, G., and Valentini, A. (2021). Recent advances of a box model to represent the estuarine dynamics: time–variable estuary length and eddy diffusivity. *J. Adv. Model. Earth Syst.* 13:e2020MS002276. doi: 10.1029/2020MS002276

Verri, G., Pinardi, N., Bryan, F., Tseng, Y.-H., Coppini, G., Clementi, E., et al. (2020). A box model to represent estuarine dynamics in mesoscale resolution ocean models. *Ocean Model.* 148:101587. doi: 10.1016/j.ocemod.2020.101587

Vezzoli, R., Mercogliano, P., Pecora, S., Zollo, A. L., and Cacciamani, C. (2015). Hydrological simulation of Po river (north Italy) discharge under climate change scenarios using the RCM COSMO-CLM. *Sci. Total Environ.* 521, 346–358. doi: 10.1016/j.scitotenv.2015.03.096

Zanchettin, D., Bruni, S., Raicich, F., Lionello, P., Adloff, F., Androsov, A., et al. (2021). Sea-level rise in Venice: historic and future trends. *Nat. Hazards Earth Syst. Sci.* 21, 2643–2678. doi: 10.5194/nhess-21-2643-2021

Appendix A: total sea level timeseries at the river mouth

To evaluate the relative role of SLR in the estuarine water exchange mechanism, a coupled atmosphere-ocean Regional Climate Model from the MedCordex framework (Cavicchia et al., 2018) was used, with ~ 10 km horizontal resolution. The daily sea level projections in a buffer area of model grid points surrounding the Po di Goro mouth were taken to represent TSL starting from 2006.

The total sea level dynamic equation is given by vertically integrating the simplified continuity equation between the sea level (η) and the seabed (H_{bathy}) and reads as below:

$$\frac{\partial \eta}{\partial t} = -\nabla \cdot ((H_{bathy} + \eta)\widehat{u}) + q_w - \frac{1}{\rho_0}\int_{-H_{bathy}}^{\eta} \frac{D\rho'}{Dt} dz' \qquad (9)$$

where the sea level variation ($\frac{\partial \eta}{\partial t}$) is composed by the divergence of the barotropic transport ($\nabla \cdot ((H_{bathy} + \eta)\widehat{u})$), with $\widehat{u}$ representing the barotropic velocity, and the surface freshwater flux ($-q_w$). These two terms are referred to as mass or incompressible terms. The last term on the right-hand side of the equation represents the thermal (thermosteric) and salinity (halosteric) contribution ($-\frac{1}{\rho_0}\int_{-H_{bathy}}^{\eta} \frac{D\rho'}{Dt} dz'$), so-called steric effect.

The RCM used here adopts the Boussinesq's approximation, i.e., meaning that the sea surface elevation includes only incompressible terms and does not account for the steric effect. Therefore, the steric sea level contribution must be added as a post-processing step. For this, the linear approximation methodology, described by Pinardi et al. (2014), was applied. The RCM considered here may underestimate the significant contribution of terrestrial ice melt entering through the Gibraltar Strait due to its coarse resolution (Galassi and Spada, 2014). Moreover, it neglects the subsidence effect, which can play a fundamental role at the local scale (Piña-Valdés et al., 2022), particularly in the northern Adriatic region (Zanchettin et al., 2021). The current sea-level observing network, alongside recent advances in process-based understanding of sea-level variability, offers the opportunity to quantify contributions from the main drivers of regional sea-level trends. Consequently, we chose to correct the long-term trend of the RCM total sea level (TSL) with the one offered by the Sea Level Evaluation and Assessment Tool (SEA Tool - https://sealevel.nasa.gov/), to obtain a more realistic sea level rise effect. This tool is supported by the NASA Sea Level Change Science Team and provides updated assessments of past, present, and future sea-level change. The projections used here are based on the assessment presented in the IPCC Sixth Assessment Report (Pörtner et al., 2022) and consider only processes for which predictions can be made with at least medium confidence. The TSL temporal variation close to the river mouth, combining RCM model variability with the long-term trend from the SEA Tool, is shown in Figure A. The trend is found to be positive through the all climate windows and with the highest value, i.e., 8 mm/yr, in the long-term range.

Appendix B: monitoring experiments to judge a site-specific NATURE-BASED Solution

The potential of halophytes to reduce the river salinity was quantified by assessing the capacity of the Atriplex portulaciodes to retain sodium (Na) from pore water. The Atriplex portulacoides responds physiologically to short-term salinity increases, making it a promising NBS for mitigating saltwater intrusion in rivers. A physical experiment was conducted at the Urban River Lab (https://urbanriverlab.com), an open-air experimental facility located at the wastewater treatment plant (WWTP) facility of Montornès del Vallès (near Barcelona, Spain). The Laboratory consists of 12 concrete flumes 12 m long × 0.6 m wide and 0.4 m deep directly fed by the WWTP water outflow. Flumes contained gravels of 10–20 mm diameter where Atriplex portulacoides (2 individuals each 50 cm) were planted for 4 months before starting the experiment. The flow rate in the flumes was 2 $lmin^{-1}$ $4\,10^{-5}$ $m^3\,s^{-1}$ and was maintained at sub-superficial level.

Atriplex portulacoides was exposed to three different salinity levels: basal (1.75), intermediate (7), and high (21) during 14 days. Each salinity level was given in three different flumes which served as replicates. To do so, we produce several solutions of water and *NaCl* (hereafter refereed as saline solution).

The saline solutions at the intermediate salinity level (i.e., 7) were pumped at a rate of 50 ml min^{-1} in the three flumes. The saline solutions at the high salinity level (21) were pumped at a flow rate of 200 ml min^{-1}. The NaCl used to produce the saline solutions has been mixed with a stirrer to ensure complete dissolution and homogenization.

Before starting the saline solution injections into the flumes, we collected samples of Atriplex portulaciodes leaves from different individuals every 2 m along each flume to determine the content of Na (Pre-sampling, T0). We repeated the same sampling procedure after 14 days of constant-rate saline solution injection in the flumes (post-sampling, T14). It is worth noting that we only considered leaves because visual inspection of plants in the flumes before starting the experiment showed that leaves were the most abundant plant compartment. T0 and T14 samplings were done on 8 March 2021 and 24 March 2021, respectively. Figure B shows the distribution of Atriplex portulacoides along a channel. We calculated total plant and leaves biomass (in $gDW\,m^{-2}$) in each flume by dividing plant or leaves dry weight (DW) by flume surface area (i.e., 7.2 m^2). The Na standing stock in leaves ($mgNa\ m^{-2}$) was determined by multiplying total leaf DW by the average Na content. Plant Na uptake, U_{plant}, measured from Na content in leaves ($mgNa\ m^{-2}$), was estimated as follows:

$$U_{plant} = \frac{LSS(14) - LSS(T0)}{\Delta T} \qquad (10)$$

where the *LSS* is the leaves *Na* standing stock, and ΔT is 14 days.

The biomass average and standard deviation (in $gDW\,m^{-2}$) of each plant compartment at the end of the study period were 64.33 ± 53.47, 38.60 ± 32.08, and 24.68 ± 20.52 $gDW\,m^{-2}$

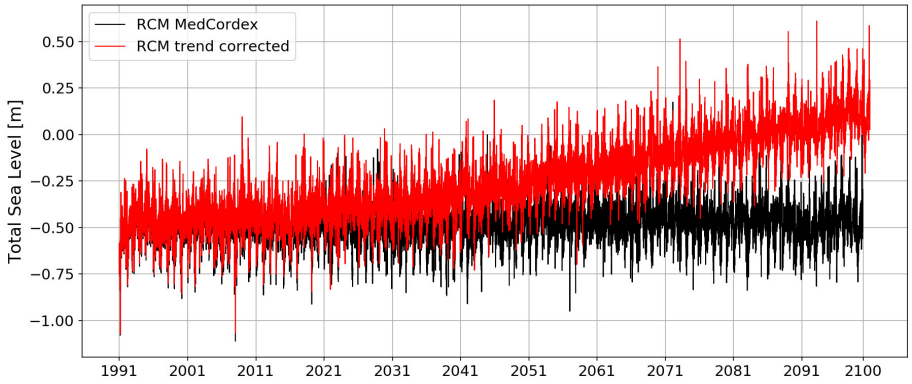

FIGURE A
Timeseries of the total sea level TSL near the Po di Goro mouth over the whole climate range 1991–2100. Black and red lines refer to the TSL computed by the RCM, before and after the trend correction, respectively.

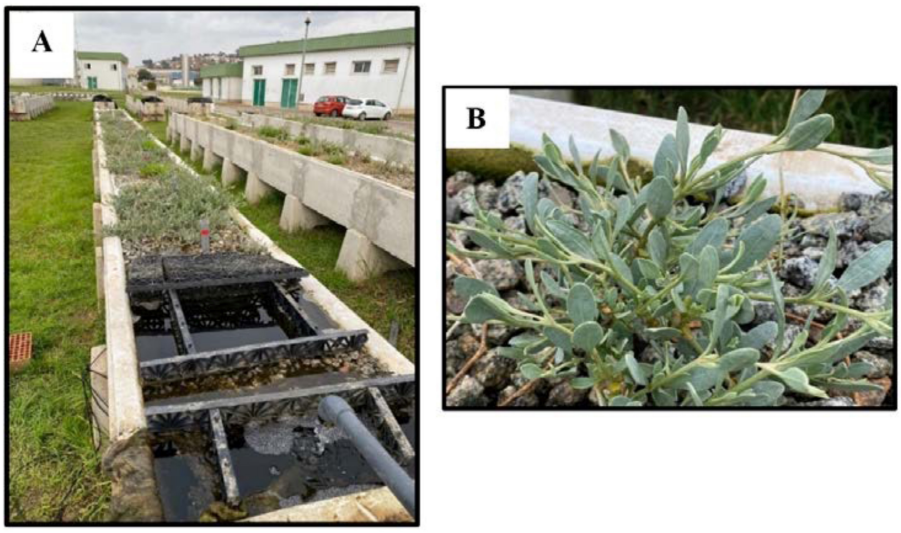

FIGURE B
General view of the Distribution of Atriplex portulacoides along a channel and **(B)** detail of **(A)**. Portulacoides and the gravel sediment.

for leaves, stems, and roots, respectively, at 1.75; 48.93 ± 19.36, 29.36 ± 11.61, and 18.78 ± 7.43 $gDW\ m^{-2}$ for leaves, stems, and roots, respectively, at 7; and 99.84 ± 37.93, 59.91 ± 22.76, and 38.31 ± 14.55 $gDW\ m^{-2}$ for leaves, stems, and roots, respectively, at 21*PSU*. Thus, as expected, leaves accounted for the highest fraction of plant biomass (50.4%).

Mean U_{plant} in flumes at 1.75 was negative, suggesting a release instead of Na uptake. Therefore, we considered that plant Na uptake at basal salinity was 0. Mean U_{plant} in flumes at intermediate and high salinity level was 5.3 and 123 $mgNa\ \ m^{-2}d^{-1}$, respectively. Overall, these results indicated that the Na uptake capacity of Atriplex portulaciodes increases according to salinity level, and this increase was not linear but exponential. Comparing the total mass of Na injected in each flume with those retained into the leaves during the 14 days of the experiment, we obtained the mean reduction (in %) of Na associated to plant uptake. Values were 0, 0.4, and 2.7% at 1.75, 7, and 21, respectively.

To scale up the results from URL to a natural ecological scale, we looked for studies that estimated leaves biomass (in $gDW\ m^{-2}$) of natural communities of Atriplex portulaciodes in South Europe. We found three studies that reported a mean leaves' biomass of 778 $gDW\ m^{-2}$ (Abbas et al., 2014; Neves et al., 2007; Valega et al., 2008) which was roughly one order of magnitude higher than those estimated at URL flumes (i.e., 71.0 $gDW\ m^{-2}$). To estimate a potential % reduction of Na from pore water in the flumes considering leaves biomass of the natural communities of Atriplex portulaciodes, we calculated the potential leaves Na standing stock ($mgNa\ m^{-2}$) in each flume after the 14 days saline solution injection considering mean leaves DW from the studies mentioned above (i.e., 778 $gDW\ m^{-2}$) and the mean leaves Na content empirically measured in the flumes at T14. This potential Na standing stock would be approximately one order of magnitude higher than the empirical estimates. Given the same total Na injection in the flumes, the potential % reduction of Na of natural

communities of Atriplex portulaciodes would be one order of magnitude higher than observed in the flumes, this is 4 and 27% at 7 and 21, respectively.

Based on these experimental levels and assuming that plants interact with 20% of the total estuary water volume, the resulting salinity entering into the channel lab when Atriplex portulacoides are planted is given by

$$S_{final} = 20\% * S_{residual} + 80\% * S_{inflow} \quad (11)$$

with

$$S_{residual} = 140 * ln(S_{inflow} + 138) - 692 \quad (12)$$

where a logarithmic law has been identified as the best curve fitting the three experimental points and providing $S_{residual}$ as a function of S_{inflow}. To note that the sodium Na and the salinity S (units of psu) reduction are considered correlated in a 1:1 relationship. The empirical law Equation 11 is used in the Experiment 3 discussed in Section 3.

Appendix C: the list of acronyms

ISS:	Inflowing Sea Salinity
RDD:	River Discharge Decrease
SLR:	Sea Level Rise
SWI:	Salt-Wedge Intrusion
NBS:	Nature-Based Solution
EBM:	Estuary Box Model
RCM:	Regional Climate Model
RCP:	Representative Concentration Pathway
TSL:	Total Sea Level